J Mater Sci (2010) 45:2015–2022
DOI 10.1007/s10853-009-4013-7

HTC2009

Surface and grain-boundary energies as well as surface mass transport in polycrystalline yttrium oxide

G. Triantafyllou · G. N. Angelopoulos · P. Nikolopoulos

Received: 9 June 2009 / Accepted: 30 October 2009 / Published online: 10 November 2009

Abstract The sessile drop technique has been used to measure the temperature dependence of the contact angle, θ, of the liquid metals Ag and Cu in contact with polycrystalline yttrium oxide (yttria, Y_2O_3) at the temperature range 1,333–1,773 K in Ar/4%H_2 atmosphere. Combination of the experimental results with literature data taken for nonwetted and nonreactive oxide/liquid metal systems permit the calculation of the surface energy of Y_2O_3 as γ_{sv} (J/m^2) = 2.278–0.391 $\times$ 10^{-3} T. For the same atmospheric conditions, thermal etching experiments on the grain boundaries intersecting the surface of the polycrystalline ceramic allow to determine the groove angles, ψ, with respect to temperature and time as well as the grain-boundary energy of Y_2O_3 as γ_{ss} (J/m^2) = 1.785–0.306 $\times$ 10^{-3} T. Grain-boundary grooving studies on polished surfaces of Y_2O_3 annealed in Ar/4%H_2 atmosphere between 1,553 K and 1,873 K have shown that surface diffusion is the dominant mechanism for the mass transport. The surface diffusion coefficient can be expressed according to the equation D_s (m^2/s) = 1.22 $\times$ 10^{-3} exp ($-343554/RT$).

Introduction

In engineering, advanced ceramics (structural or functional) considered to be the most suitable for use in high temperature applications, while a special interest is being manifested in the compounds of ceramics with metals and metal alloys.

G. Triantafyllou · G. N. Angelopoulos · P. Nikolopoulos (✉)
Department of Chemical Engineering, University of Patras, 26504 Patras, Greece
e-mail: nikolop@chemeng.upatras.gr

Yttrium oxide (Y_2O_3) is a material used in functional and structural applications. Y_2O_3 additives in ZrO_2 stabilizes the high temperature cubic phase with fluorite structure of ZrO_2 (YSZ), which shows a high ionic conductivity for use as electrolyte in a variety of electrochemical applications (high temperature solid oxide fuel cells—SOFCs [1], oxygen sensors [2]) as well as in combination with a metal (Ni–cermet) as anode electrode in SOFCs. Furthermore, Y_2O_3 partially stabilized ZrO_2 (YPZ) with tetragonal precipitates, shows high fracture toughness and good thermal shock resistance, which makes it suitable for applications as industrial wear parts, cutting tools as well as heat engines and biomedical ceramics. Due to its good adhesion properties in contact with glasses, different metals, and compounds [3], Y_2O_3 can serve as an adherence promoter for multilayer coatings. Surface and interfacial energies of Y_2O_3 are often required for the theoretical treatment of a number of phenomena, such as strength, nucleation, sintering behavior, and mass transport.

An established method for studying the interfacial phenomena is that of a sessile drop of a liquid lying on the surface of a solid substrate (Fig. 1a). In thermodynamic equilibrium, the Young equation is valid:

$$\gamma_{sv} = \gamma_{sl} + \gamma_{lv} \cos\theta, \quad (1)$$

where γ_{sv} and γ_{lv} are the surface energies of the solid and the liquid, respectively, γ_{sl} is the interfacial energy of solid–liquid and θ is the contact angle.

For a nonwetting ceramic/metal system, the contact angle as well as the surface energy of the liquid metal can be evaluated from sessile drop experiment. The determination of the surface energy of the oxide as well as of the interfacial energy of the system requires the application of a combination of experimental methods (multiphase equilibration technique [4–9]) or indentation techniques

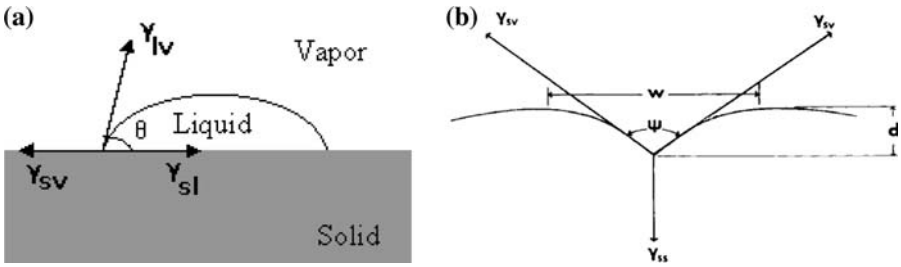

Fig. 1 Schematic profiles showing **a** contact angle, θ, in a solid–liquid–vapor system and **b** a thermally etched grain-boundary groove

[10]. For this reason, most of the literature data were derived from theoretical evaluations [11].

When a grain-boundary intersects a solid surface, a groove tends to be formed along the line of intersection at temperatures higher than half of the absolute melting point of the material [12]. At equilibrium, the established groove angle, ψ, at the root of groove (Fig. 1b), depends on the ratio of the grain-boundary energy, γ_{ss}, to the surface energy, γ_{sv}, of the polycrystalline solid according the relationship

$$\gamma_{ss} = 2\gamma_{sv}\cos(\psi/2). \quad (2)$$

The groove progressively grows by preferential atomic migration, by either diffusion or evaporation. For a grain-boundary perpendicular to the surface with a groove width initially equal to the grain-boundary groove shoulder, w, the groove can grow with time, t, by several mechanisms. According to Mullins's theory for thermal grooving [13], for a surface diffusion mechanism, the width, w, (Fig. 1b) is given by

$$w = 4.6(Bt)^{1/4} \quad (3)$$

with

$$B = D_s N\Omega^2\gamma_{sv}/kT, \quad (4)$$

where D_s is the surface diffusion coefficient, Ω and $N = \Omega^{-2/3}$ are the molar volume and the surface density of the diffusing species, respectively, k is the Boltzmann constant, and T is the temperature.

The aim of this study is the determination of the temperature dependence of the surface and grain-boundary energies of polycrystalline Y_2O_3 in Ar/4%H_2 atmosphere as well as the mass transport phenomena across the Y_2O_3 surface at the temperature range 1,553–1,873 K.

Experimental

The round discs of 20 mm diameter and 2 mm thickness of polycrystalline Y_2O_3 used in the experiments were prepared via cold pressing and sintering of commercially available powders (MTI Corporation) with a purity of 99.99% (impurities in ppm: rare earths: Eu $<$ 4.9, rest $<$ 0.5 and common metals: Ce $<$ 10, Fe = 2, Cu = 2, Si = 28, Ni = 3, Pb = 2), mean particle size $\approx$ 8 μm, and density $\rho = 5.013$ g/cm^3. The samples were sintered at 1,923 K for 30 h to a density 90% of the theoretical. All the samples were metallographically polished to a final roughness of $<$0.3 μm. The metallic phase used was Ag-rods (purities in ppm: Cu = 17, Fe = 2, and Pb = 1) and Cu-rods (Alfa Aesar GmbH) with a purity of 99.95% and 99.999%, respectively.

The sessile drop experiments were performed in a horizontal inductive furnace coupled with a molybdenum susceptor in flowing Ar/4%H_2 atmosphere (90 mL/min). Optical windows permitted the in situ observation of the experiment using a video-camera system, as well as the measurement of the temperature by optical pyrometry with a precision of about ±5 K. The equilibrium contact angle, θ, was established during the first minutes of the experiments and remained constant for the whole experimental time (20 min).

The thermal etching experiments were performed in a SiC resistance furnace in flowing Ar/4%H_2 atmosphere, where the specimens were supported in an alumina tube. Similar experiments were also performed in flowing Ar-atmosphere and in air. Optical interferometry, using a Leitz interferometer with a resolution limit of 0.3272 μm, was applied to the measurements of the groove angle, ψ, and groove width, w (Fig. 1b). Since it is difficult to discriminate between grain boundaries that do not intercept perpendicular to the surface plane section, only those angles in which the interference pattern continued in approximately the same manner on both sides of the groove were considered (Fig. 2). The true root angle, ψ, was calculated using the equation [14]

$$\tan(\psi/2) = 2\delta\tan(\alpha/2)/1.11\lambda m, \quad (5)$$

where α and δ are the apparent root angle and the fringe spacing, respectively, measured from the interferometric patterns shown in Fig. 2, λ is the wave length of the light source ($\lambda_{Na} = 589$ nm), and m is the magnification. The factor 1.11 is a correction factor for the effect of the large aperture of the lens. The duration of the experiments had to be chosen so as to allow the grooves to obtain measurable dimensions of depth, d, and width, w, of the groove shoulders.

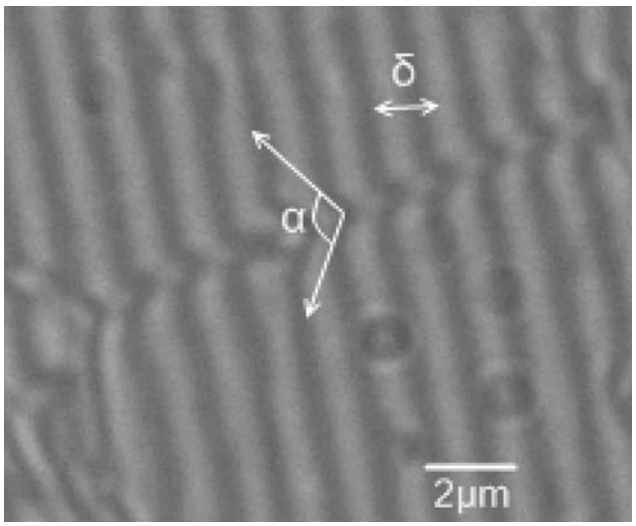

Fig. 2 Interference patterns to obtain groove angle, ψ, of Y_2O_3 in Ar/4%H_2 at $T = 1{,}693$ K and $t = 50$ h (α = apparent angle and δ = fringe spacing)

For the calculation of the molar volume, Ω, and the surface density, N, (Eq. 4) at high temperatures, the linear thermal expansion coefficient (TEC) of Y_2O_3 was measured in the temperature range 298–1,673 K, using a high temperature push-rod dilatometer (Fa. Netzsch).

In all experiments carried out in Ar/4%H_2 with a moisture content of about 10 vpm, the oxygen partial pressure, $P(O_2)$, was in the range 1.4×10^{-21} to 6.4×10^{-16} with increasing temperature between 1,333 and 1,873 K. Under these conditions, thermodynamic data show that Y_2O_3 keep its stability in the whole temperature range examined. The low oxygen partial pressure in the furnace atmosphere does not influence the surface energy values of the liquid metals Ag [15, 16] and Cu [17–19] at their melting points, neither their temperature dependence.

Surface and grain-boundary energies

Theoretical treatment

Table 1 includes literature data [4–11, 20–29] concerning linear temperature dependencies of the surface energy of different oxides and liquid metals as well as the contact angle values between the liquid metals Sn, Cu, Ni and Fe and the various oxides at 1,173, 1,400, 1,773, and 1,823 K, respectively. The contact angle values are either average literature values referring to the given temperatures or have been derived from interpolation of experimental data assuming linear temperature dependence. All systems examined are nonwetting and nonreactive under inert, vacuum, or reducing atmospheric conditions. The values of the contact angle as well as of the surface and interfacial energies hardly depend on the dissolved oxygen of the oxides in the liquid metals [30, 31]. In particular, the low partial pressure of dissolved oxygen in the metals Sn, Cu, Ni, and Fe does not influence their surface energy, according data given by Saiz et al. [32].

According to the data given in Table 1, the interfacial energy, γ_{sl}, of the oxides/liquid metal systems can be calculated using Eq. 1. The results show that the interfacial energy values between a metal and the various oxides with which is in contact, follows an approximately linear relationship with cos θ at a given temperature (Fig. 3). For the tested systems and $\theta > 90°$, the following relations were obtained.

(a) Oxides/Sn at 1,173 K (Fig. 3a)

$$\gamma_{sl}\ (\mathrm{J/m^2}) = -4.342\cos\theta - 0.982, \quad R^2 = 0.934 \qquad (6a)$$

(b) Oxides/Cu at 1,400 K (Fig. 3b)

$$\gamma_{sl}\ (\mathrm{J/m^2}) = -4.149\cos\theta - 0.513, \quad R^2 = 0.984 \qquad (6b)$$

(c) Oxides/Ni at 1,773 K (Fig. 3c)

$$\gamma_{sl}\ (\mathrm{J/m^2}) = -3.781\cos\theta + 0.038, \quad R^2 = 0.944 \qquad (6c)$$

(d) Oxides/Fe at 1,823 K (Fig. 3d)

$$\gamma_{sl}\ (\mathrm{J/m^2}) = -3.708\cos\theta + 0.294, \quad R^2 = 0.905 \qquad (6d)$$

Correlations (6a) to (6d) obey the general equation:

$$\gamma_{sl}\ (\mathrm{J/m^2}) = A\cos\theta + B \qquad (7)$$

In the investigated temperature range 1,173–1,823 K, the slope A, and the constant B (Eq. 7) satisfy the following linear dependence on temperature:

$$A\ (\mathrm{J/m^2}) = 0.970 \times 10^{-3}\ \mathrm{T} - 5.491 \quad R^2 = 0.998 \qquad (8)$$

$$B\ (\mathrm{J/m^2}) = 1.825 \times 10^{-3}\ \mathrm{T} - 3.106 \quad R^2 = 0.984. \qquad (9)$$

Introducing Eq. 7 to Eq. 1 gives:

$$\gamma_{sv}\ (\mathrm{J/m^2}) = (A + \gamma_{sv})\cos\theta + B. \qquad (10)$$

According to Eq. 10 in a nonwetting and nonreactive oxide/liquid metal system, at a given temperature, the surface energy of the oxide can be calculated from the surface energy of the liquid metal and the measured contact angle value, or, conversely, the expected contact angle can be estimated for a given value of the surface energy of the oxide.

Surface energy

In order to determine the surface energy of Y_2O_3 as well as its temperature dependence, wetting experiments were performed in the systems Y_2O_3/Ag and Y_2O_3/Cu at the temperature range 1,333–1,763 K and 1,483–1,773 K,

Table 1 Temperature dependence of the surface energy of solid oxides, γ_{sv}, and liquid metals, γ_{lv}, as well as contact angle values, θ, in oxide/liquid metal systems

Oxide	Surface energy of solid oxides γ_{sv} (J/m^2)	Oxides/Sn at 1,173 K θ (°)	Oxides/Cu at 1,400 K θ (°)	Oxides/Ni at 1,773 K θ (°)	Oxides/Fe at 1,823 K θ (°)
Al_2O_3	2.559–0.784 × 10^{-3} T [6]	135 [6, 20]	134 [19, 24]	119 [24]	131 [24, 27]
BeO	2.400–0.359 × 10^{-3} T [11]			149 [27]	137 [27]
MgO	2.600–0.476 × 10^{-3} T [11]	139 [21]	152 [21]	142 [27]	130 [27]
CaO	2.200–0.381 × 10^{-3} T [11]			139 [21]	132 [25]
$MgAl_2O_4$	3.000–0.577 × 10^{-3} T [11]	147[a]	155 [21]	156 [21]	134 [21]
ThO_2	1.562–0.240 × 10^{-3} T [10]			133 [27]	112 [27]
UO_2	1.507–0.346 × 10^{-3} T [5]	119 [22]	120 [4, 22, 25]	112 [5]	
CSZ	1.428–0.431 × 10^{-3} T [7]	123 [23]	126 [26]	120 [26]	115 [29]
YSZ	1.927–0.428 × 10^{-3} T [8]	130 [8]		117 [28]	
CeO_2	2.465–0.563 × 10^{-3} T [9]	138[a]	143 [9]	127[a]	
TiO_2	0.800–0.167 × 10^{-3} T [11]			105 [27]	92 [27]
Surface energy of liquid metals (J/m^2) [24]					
Sn: $\gamma_{lv} = 0.544–0.07 \times 10^{-3} (T - T_m)$, $T_m = 505$ K			Ni: $\gamma_{lv} = 1.754–0.28 \times 10^{-3} (T - T_m)$, $T_m = 1{,}726$ K		
Cu: $\gamma_{lv} = 1.311–0.20 \times 10^{-3} (T - T_m)$, $T_m = 1{,}356$ K			Fe: $\gamma_{lv} = 1.825–0.27 \times 10^{-3} (T - T_m)$, $T_m = 1{,}809$ K		

[a] This work

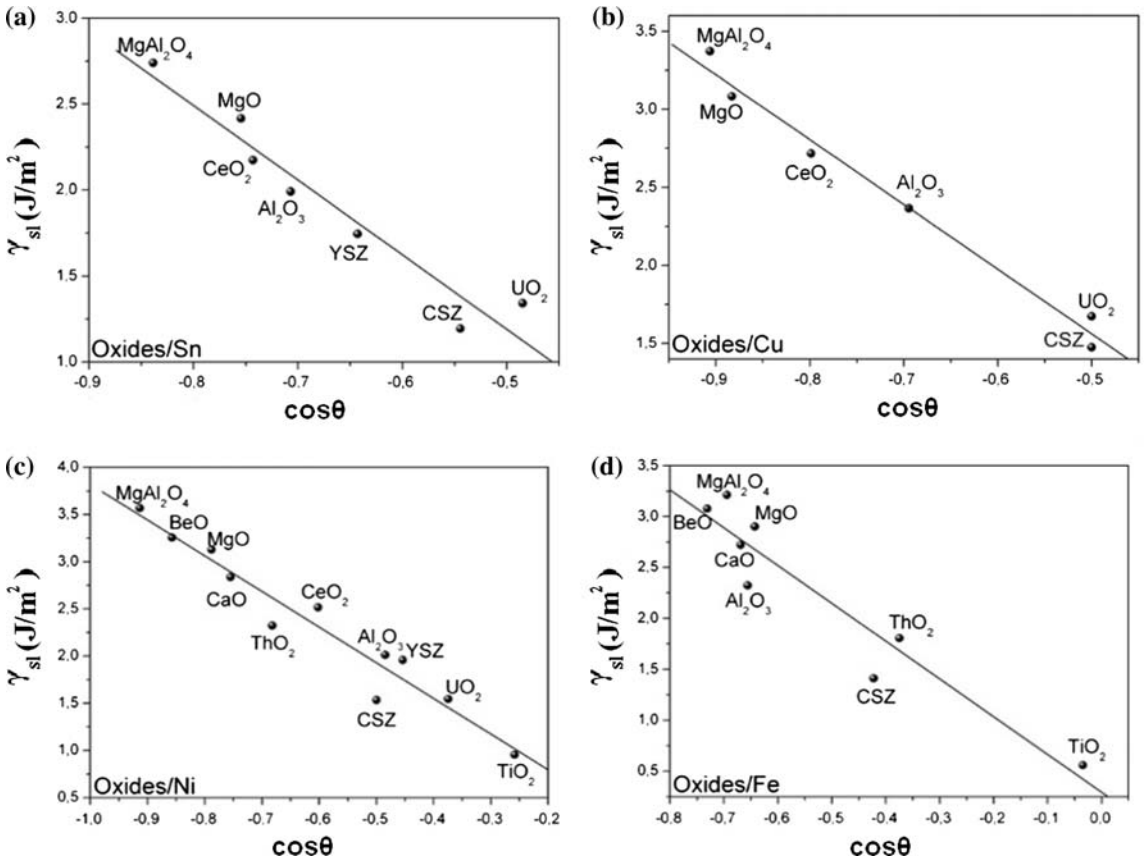

Fig. 3 Interfacial energy, γ_{sl}, versus cosθ in systems of oxides in contact with **a** Sn at 1,173 K, **b** Cu at 1,400 K, **c** Ni at 1,773 K, and **d** Fe at 1,823 K

respectively, in Ar/4%H_2 atmosphere. Table 2 includes the measured contact angle values as well as the temperature dependence of the surface energy of the liquid metals. The mean contact angles, θ (Table 2), with a standard error of about ±2°, as a mean deviation of three different wetting experiments, indicate nonwetting ($\theta > 90°$) conditions at

Table 2 Temperature dependence of contact angle, θ, in the Y_2O_3/Ag and Y_2O_3/Cu systems

Y_2O_3/Ag		Y_2O_3/Cu	
T (K)	θ (deg)	T (K)	θ (deg)
1,333	137.5	1,483	139.2
1,383	135.5	1,548	135.9
1,443	133.0	1,628	132.2
1,473	131.7	1,688	129.0
1,513	130.0	1,725	127.2
1,553	128.5	1,773	124.8
1,573	127.5		
1,623	125.5		
1,653	124.4		
1,713	122.2		
1,763	120.4		
Surface energy of liquid metals (J/m^2) [24]			
$\gamma_{lv} = 0.912–0.15 \times 10^{-3}$ $(T - T_m)$, $T_m = 1{,}234$ K		$\gamma_{lv} = 1.311 - 0.2 \times 10^{-3}$ $(T - T_m)$, $T_m = 1{,}356$ K	

the oxide/liquid metals interface. SEM–EDS analysis on the cross sections of the samples after wetting experiments shows no interaction at the oxide/metal interface.

At a given temperature, inserting the data of cos θ and γ_{lv} (Table 2) as well as the values of A (Eq. 8) and B (Eq. 9) in Eq. 10 the surface energy of the Y_2O_3 can be calculated. The results (Fig. 4) show a nearly linear temperature dependence of the surface energy of Y_2O_3, satisfying following relation:

$$\gamma_{sv}\ (\mathrm{J/m^2}) = 2.278 - 0.391 \times 10^{-3}\ \mathrm{T}, \quad R^2 = 0.987. \tag{11}$$

The lack of experimentally determined surface energy values in the literature does not allow the comparison with our results. For calculations at high temperatures, the estimated value, $\gamma_{sv} = 1.0$ J/m^2, is typically used [33]. The

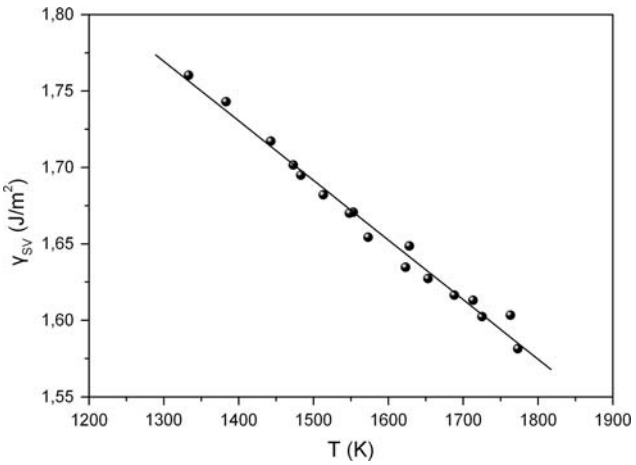

Fig. 4 Temperature dependence of the surface energy of Y_2O_3

temperature coefficient of the surface energy or surface entropy term ($d\gamma_{sv}/dT = 0.391 \times 10^{-3}$ J m^{-2} K^{-1}), compares well with the corresponding values of other oxides, particularly for those with similar crystal structure (Table 1).

Inserting the results shown in Table 2 in Eq. 7, the temperature dependence of the interfacial energies in the systems Y_2O_3/Ag (Eq. 12) and Y_2O_3/Cu (Eq. 13) is found to be given by the following equations:

$$\gamma_{sl}\ (\mathrm{J/m^2}) = 2.512 - 0.952 \times 10^{-3}\ (\mathrm{T} - 1{,}234\ \mathrm{K}), \quad R^2 = 0.996 \tag{12}$$

$$\gamma_{sl}\ (\mathrm{J/m^2}) = 2.842 - 1.329 \times 10^{-3} (\mathrm{T} - 1{,}356\ \mathrm{K}), \quad R^2 = 0.998. \tag{13}$$

The calculated absolute values of the temperature coefficient of surface energy of the oxide, γ_{sv} (Eq. 11), interfacial energies, γ_{sl} (Eqs 12 and 13) as well as the surface energy of the liquid metal, γ_{lv} (Table 2), show that for an oxide/liquid metal system $d\gamma_{sl}/dT > d\gamma_{sv}/dT + d\gamma_{lv}/dT$. Due to the fact that, in the wettability performance the quantities γ_{sl}, γ_{sv} and γ_{lv} act together, decreasing the interfacial energy, γ_{sl}, with temperature leads to lower contact angle values and therefore of the bond strength at the Y_2O_3/liquid metal interface. Furthermore, in systems of an oxide in contact with different liquid metals the value $d\gamma_{sl}/dT$ increases with increasing $d\gamma_{lv}/dT$ of the metal, in accordance with literature data for CSZ [23] and Al_2O_3 [24]/liquid metal systems.

Grain-boundary energy

In order to determined the grain-boundary energy of Y_2O_3 (Eq. 2), the groove angle, ψ, was measured after thermal etching experiments at 1,553 K for 70, 90, and 110 h, at 1,623 K for 45, 60, 75, and 105 h, at 1,693 K for 50, 60, 90, and 100 h, at 1,773 K for 3, 5, and 9 h and at 1,873 K for 3, 5, and 7 h in Ar/4%H_2 and for comparison some of them in Ar and air. In this study, it is assumed, in accordance with literature [34], that the surface energy of polycrystalline Y_2O_3 is independent of crystallographic orientations and the mean value of, ψ, is not influenced by the presence of grain-boundary torque-term effects caused by surface energy anisotropy.

The statistical tests of the results, which concern the time and furnace atmosphere mean groove angle, ψ, values, show that they can be considered as random samples of the same distribution at a given temperature and, therefore, they are practically independent of the annealing time and atmosphere. In the first case, this fact leads to the conclusion that the increase of the groove depth, d, follows the same relation with time as the width of the groove shoulders, w (Fig. 1b), which agrees with Mullins's theory [13].

Table 3 Groove angle, ψ, and ratio, γ_{ss}/γ_{sv}, in thermally etched polycrystalline Y_2O_3

T (K)	Number of angles	ψ (°)			γ_{ss}/γ_{sv}	
		Range	Mean value	Std. error of mean	Mean value	Std. error of mean
1,553	590	126.3–141.9	134.0	±0.1	0.782	±0.002
1,623	616	124.3–143.5	133.8	±0.1	0.786	±0.001
1,693	536	121.9–144.7	133.9	±0.1	0.783	±0.002
1,773	565	123.4–142.5	133.8	±0.1	0.784	±0.002
1,873	466	122.0–145.1	134.0	±0.1	0.782	±0.002

The number of measured grain-boundary groove angles in polycrystalline Y_2O_3, the distribution interval of single ψ values and the mean ψ values, as well as the ratio γ_{ss}/γ_{sv}, depending on temperature is summarized in Table 3. The difference between the minimum and the maximum ψ values is a measure of the misorientation of the grain-boundary grooves, relative to the normal, that intersect the free surface of Y_2O_3. Introducing the results (Eq. 11, Table 3) in Eq. 2, the temperature dependence of the grain-boundary energy of Y_2O_3 is calculated as:

$$\gamma_{ss}\ (\mathrm{J/m^2}) = 1.785 - 0.306 \times 10^{-3}\ \mathrm{T}, \quad R^2 = 0.992. \tag{14}$$

The temperature coefficient of the grain-boundary energy ($\mathrm{d}\gamma_{ss}/\mathrm{d}T = 0.306 \times 10^{-3}$ J m^{-2} T^{-1}) given in Eq. 14 is in agreement with the corresponding values (0.193×10^{-3} J m^{-2} T^{-1}) for UO_2 [5], (0.392×10^{-3} J m^{-2} T^{-1}) for calcia-stabilized zirconia (CSZ) [7], and (0.358×10^{-3} J m^{-2} T^{-1}) for yttria-stabilized zirconia (YSZ) [8] of oxides with cubic structure. Taking into account the fluctuation of the solitary values of ψ (Table 3), a mean groove angle $\psi^{m} = 133.9° \pm 0.05°$ can be determined, leading to a mean value of the ratio, $\gamma_{ss}/\gamma_{sv} = 0.783 \pm 0.001$, which is independent of the experimental conditions.

The value of the ratio (γ_{ss}/γ_{sv}) is important for the prediction of sintering behavior and the properties of powder consolidated oxides. The present result of the ratio γ_{ss}/γ_{sv} between 0.782 and 0.785 for Y_2O_3 is in agreement with respective values reported in the literature (optical methods) for ionic bonded ceramics such as UO_2 (0.54–0.67 [4], 0.54–0.58 [5], 0.45 [35]), Al_2O_3 (0.696–0.738 [6], 0.707 [34], 0.54 [36]), CSZ (0.45–0.53 [7]), YSZ (0.487–0.534 [8]), and CeO_2 (0.677–0.679 [9]). The above results indicate that for the oxides the expected grain-boundary energy values are in the range $0.5\gamma_{sv} < \gamma_{ss} < \gamma_{sv}$, whereas for metals $\gamma_{ss} \sim 0.33\ \gamma_{sv}$.

Surface diffusion coefficient

In parallel with the measurement of the groove angle, ψ, the corresponding value of groove width, w (Fig. 1b) was also measured as a function of time and temperature in Ar/4% H_2 (Table 4). Corresponding experiments carried out in Ar and air at the same temperature and time intervals showed no changes in the groove widths.

Table 4 Groove width, w, in thermally etched polycrystalline Y_2O_3 at different temperatures and times

T (K)	t (h)	w (μm)	
		Average width[a]	Std. error of mean
1,553	70	0.905	0.007
	90	0.986	0.007
	110	1.011	0.008
	130	1.029	0.009
1,623	45	0.872	0.004
	60	0.933	0.006
	75	0.969	0.006
	105	1.016	0.008
1,693	50	1.062	0.006
	60	1.088	0.010
	90	1.136	0.011
	100	1.178	0.007
1,773	3	0.901	0.007
	5	0.990	0.009
	7	1.062	0.009
	9	1.105	0.009
1,873	3	1.069	0.009
	5	1.281	0.008
	7	1.335	0.010

[a] Measured widths, w, for each time interval were ≈ 140

The slopes of the lines log w versus log t (Fig. 5) vary between 0.16 and 0.27 with a mean value of 0.20, which agrees with the slopes 0.16–0.29 [34], 0.17–0.20 [36], 0.24 [37] for Al_2O_3, 0.23–0.27 for MgO [38], and 0.24–0.26 for CeO_2 [9]. In all of these cases, the values are close to 0.25 that Mullins [13] proposes, for surface diffusion as the predominant mechanism of grain-boundary grooving, which is used for the calculation of the surface diffusion coefficient in the temperature ranges studied. Furthermore, from the measured mean groove angle, $\psi = 133.9°$, the slope of the grain-boundary profile with respect to the flat

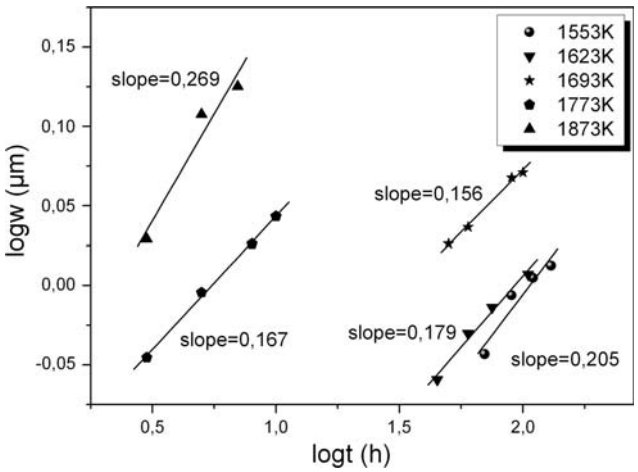

Fig. 5 Groove widths, w, at the solid–vapor surface of polycrystalline Y_2O_3 as a function of time, t, for different temperatures

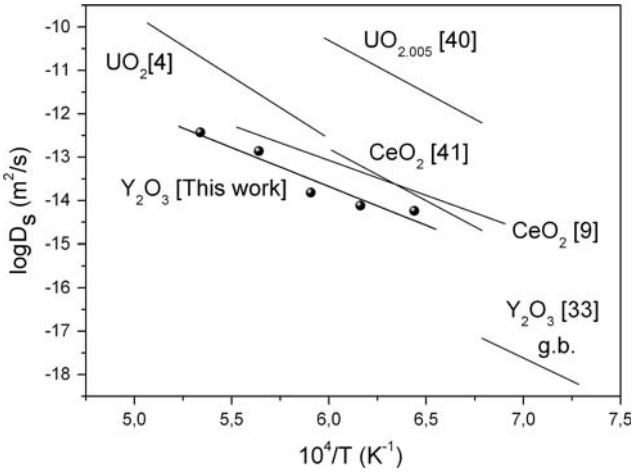

Fig. 6 Arrhenius plots of surface diffusion coefficients of various oxides and grain-boundary (g.b.) diffusion coefficient of Y_2O_3

surface, $\tan(90 - \psi/2) = 0.426$, justifies the small slope approximation for the groove width (Eq. 3), with an accuracy of about 20% for the surface diffusion coefficient according the analysis given by Robertson [39].

By combining Eqs. 3 and 4, D_s is given by

$$D_s = w^4 kT/4.6^4 \gamma_{sv} \Omega^2 Nt, \quad (15)$$

where the data for γ_{sv} and w, t are available from Eq. 11 and Table 4, respectively, $k = 1.38062 \times 10^{23}$ J/K and $\Omega = 3.742 \times 10^{-29}$ m^3/molecule, considered as one-half of the Y_2O_3 molecule in an Y_2O_3 crystal, since it is not known what species is diffusing [34] and, therefore, $N = \Omega^{-2/3} = 8.938 \times 10^{18}$ molecules/m^2, at room temperature. In order to calculate the temperature dependence of molar volume as well as of the surface density, the linear TEC of Y_2O_3 at the temperature range 298–1,673 K was determined as $\alpha = 8.56 \times 10^{-6}$ K^{-1}. Assuming isotropic material, the volume expansion coefficient can be considered as 3α. From the calculated values (Eq. 15), the surface self-diffusion coefficient of Y_2O_3 in Y_2O_3 can be expressed by the relation:

$$D_s\ (\mathrm{m}^2/\mathrm{s}) = 1.22 \times 10^{-3} \exp(-343554/RT). \quad (16)$$

Figure 6 illustrates the Arrhenius plot of the surface diffusion values of cubic C-type crystal structure of Y_2O_3 (deriving from the fluorite-type cubic structure with one-fourth of the anion sites vacant and regularly arranged), together with literature data for fluorite structured oxides UO_2 [4, 40] and CeO_2 [9, 41], measured via grain-boundary grooving, as well as data for grain-boundary diffusion in Y_2O_3 [33], measured via grain growth (Table 5). The value of D_o for the grain-boundary diffusion, is estimated from the value $bD_o = 2.36 \times 10^{-12}$ [33], assuming a grain-boundary width of about $b \sim 1$ nm.

The D_s values for the stoichiometric oxides (Fig. 6), obtained at the same temperature interval, are distributed in a narrow range of about one to two orders of magnitude. This can be attributed to the fact that the diffusion process refers to the transfer of mass in which the transport corresponds to movement of groups of coupled atoms to prevent composition fluctuations [40].

Results obtained for surface diffusion of Y_2O_3 (Fig. 6) at low-temperature ranges ($T < 1{,}623$ K) present values for both D_o and E_s lower than those obtained at high temperature ranges, indicating the probability of two distinct zones of diffusion. Similar behavior has been observed by Berard and Wilder [42] in a study for Y^{3+} self-diffusion in fully dense polycrystalline Y_2O_3. A possible reason for this behavior is the structural damage that mechanical polishing causes to the near-surface region of the specimen, enhancing the dislocation density and consequently the diffusion process, without changing the diffusion mechanism and the mass transport (structure-sensitive extrinsic surface diffusion) [34]. Furthermore, the results (Table 5) show that in polycrystalline Y_2O_3, $E_s < E_{gb}$, and extrapolating the D_s-values, at lower temperatures, that $D_s > D_{gb}$ (Fig. 6).

Conclusions

Wetting experiments in the nonwetting and nonreactive systems of Y_2O_3/Ag and Cu were used to determine the surface energy, γ_{sv}, of polycrystalline Y_2O_3 according to the determined relationship $\gamma_{sv} = (A + \gamma_{lv})\cos\theta + B$, with A and B linear temperature functions. The measurements of the contact angle, θ, were performed in Ar/4%H_2 at the temperature range 1,333–1,773 K. The calculated surface energy values for Y_2O_3 satisfy the following relationship:

Table 5 Surface diffusion data of various oxides and grain-boundary diffusion data for Y_2O_3

Oxides	Atmosphere	T (K)	D_0 (m^2/s)	E (kJ/mol)	Reference
Surface diffusion					
UO_2	Ar	1,673–1,973	4×10^4	548.0	[4]
$UO_{2.005}$	Ar	1,473–1,673	1.3×10^4	460.5	[40]
CeO_2	Ar	1,473–1,773	3.82×10^{-4}	308.3	[9]
CeO_2	Air	1,473–1,663	35	458.0	[41]
Y_2O_3	Ar/4%H_2	1,553–1,873	1.22×10^{-3}	343.6	This work
Grain-boundary diffusion					
Y_2O_3	Air	1,373–1,473	2.36×10^{-3}	410	[33]

$$\gamma_{sv}\ (J/m^2) = 2.278 - 0.391 \times 10^{-3}\ T$$

Thermal etching experiments and groove angle, ψ, measurements were used to calculate the temperature dependence of the grain-boundary energy of Y_2O_3 in the range 1,573–1,873 K.

$$\gamma_{ss}\ (J/m^2) = 1.785 - 0.306 \times 10^{-3}\ T.$$

Statistical tests have shown that the ψ values can be considered as random samples of the same distribution, giving values for the mean groove angle, ψ^m, and the mean ratio, γ_{ss}/γ_{sv}, of 133.9° and 0.783, respectively, independent of annealing atmosphere, time, and temperature.

Surface diffusion, as mass-transport mechanism of coupled groups of atoms, is responsible for grain-boundary grooving in polycrystalline Y_2O_3, with coefficient D_s (m^2/s) $= 1.22 \times 10^{-3} \exp(-343554/RT)$. At the low temperature region, about a half of the melting point of Y_2O_3, a structure-sensitive extrinsic surface diffusion can be observed, without influence on the mechanism of diffusion process and the equilibrium mean values of the formed groove angles.

Acknowledgements Financial support by the 6th Framework Program, STRP 033410 MATSILC Project, is gratefully acknowledged.

References

1. Boudghene Stambouli A, Traversa E (2002) Renew Sust Energ Rev 6:433
2. Rodrigues CMS, Labrincha JA, Marques FMB (2000) Solid State Ionics 136–137:671
3. Kim D, Jeong S, Moon J, Cho SH (2006) J Colloid Interface Sci 297:589
4. Hodkin EN, Nicholas MG (1973) J Nucl Mater 47:23
5. Nikolopoulos P, Nazare S, Thümmler F (1977) J Nucl Mater 71:89
6. Nikolopoulos P (1985) J Mater Sci 20:3993. doi:10.1007/BF00552390
7. Sotiropoulou D, Nikolopoulos P (1991) J Mater Sci 26:1395. doi:10.1007/BF00544484
8. Tsoga A, Nikolopoulos P (1996) J Mater Sci 31:5409. doi:10.1007/BF01159310
9. Zouvelou N, Mantzouris X, Nikolopoulos P (2008) Mater Sci Eng A 495:54
10. Inoue T, Matzke Hj (1981) J Am Ceram Soc 64:355
11. Bruce RH (1965) In: Stewart GH (ed) Science of ceramics, vol 2. Academic press, London
12. Allen BC (1969) Trans Metall Soc AIME 245:1621
13. Mullins WW (1957) J Appl Phys 28:333
14. Amelinckx S, Binnendijk NF, Dekeyser W (1953) Physica XIX:1173
15. Sangiorgi R, Muolo ML, Passerone A (1982) Acta Metall 30:1597
16. Chatain D, Chabert F, Ghetta V (1994) J Am Ceram Soc 77:197
17. Gallois B, Lupis CHP (1981) Metall Trans B 12:549
18. Mehrotra SP, Chaklader ACD (1985) Metall Trans B 16:567
19. Ghetta V, Fouletier J, Chatain D (1996) Acta Mater 44:1927
20. Rivollet I, Chatain D, Eustathopoulos N (1987) Acta Metall 35:835
21. Zagar L, Bernhardt W (1966) Forschungsberichte des Landes Nordrhein-Westfalen, Nr. 1733, Westdeutscher Verlag, Köln
22. Livey DT, Murray P (1956) The wetting properties of solid oxides and carbides by liquid metals. In: 2nd Plansee seminar. Springer Verlag, Wien, pp 375–404
23. Nikolopoulos P, Ondracek G, Sotiropoulou D (1989) Ceram Int 15:201
24. Nikolopoulos P, Agathopoulos S (1992) J Eur Ceram Soc 10:415
25. Naidich JV (1981) In: Cadenhead DA, Danielli (eds) Progress in surface and membrane science, vol 14. Academic press, New York, pp 353–484
26. Nikolopoulos P, Sotiropoulou D (1987) J Mater Sci Lett 6:1429
27. Humenik M, Kingery WD (1954) J Am Ceram Soc 37:18
28. Tsoga A, Naoumidis A, Nikolopoulos P (1996) Acta Mater 44:3679
29. Sotiropoulou D, Nikolopoulos P (1993) J Mater Sci 28:356. doi:10.1007/BF00357807
30. Eustathopoulos N, Nicholas MG, Drevet B (1999) In: Cahn RW (ed) Wettability at high temperatures, vol 3. Pergamon Materials Series, Amsterdam
31. Zouvelou N, Mantzouris X, Nikolopoulos P (2007) Int J Adhes Adhes 27:380
32. Saiz E, Cannon RM, Tomsia AP (2008) Annu Rev Mater Res 38:197
33. Wang XH, Chen PL, Chen IW (2006) J Am Ceram Soc 89:431
34. Tsoga A, Nikolopoulos P (1994) J Am Ceram Soc 77:954
35. Bratton RJ, Beck CW (1971) J Am Ceram Soc 54:379
36. Shackelford JF, Scott WD (1968) J Am Ceram Soc 51:688
37. Gaddipati AR, Scott WD (1986) J Mater Sci 21:419. doi:10.1007/BF01145503
38. Lytle SA, Stubican VS (1982) J Am Ceram Soc 65:210
39. Robertson WM (1971) J Appl Phys 42:463
40. Henney J, Jones JWS (1968) J Mater Sci 3:158. doi:10.1007/BF00585483
41. Jin M, Shimada E, Ikuma Y (2000) J Ceram Soc Jpn 108:456
42. Berard MF, Wilder DR (1969) J Am Ceram Soc 52:85